


Effect of Protein and Mechanical Strain on the Corrosion Resistance and Cytotoxicity of the Orthodontic Composite Arch Wire

Longwen He, Ye Cui, and Chao Zhang*

 Cite This: *ACS Omega* 2020, 5, 8992–8998

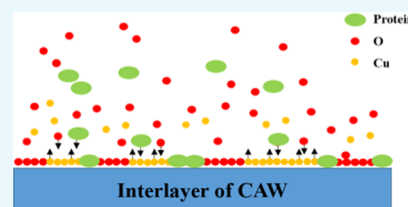
 Read Online

ACCESS |

 Metrics & More

 Article Recommendations

ABSTRACT: In this study, the effects of the exposure to different types of salivary proteins (fibrinogen, IgG, and mucin) and application of an in vitro bending strain on the laser welding orthodontic composite arch wire (CAW) were investigated, and the resultant corrosion behavior and cytotoxicity were studied in vitro. The purpose was to determine the mechanisms by which protein exposure and bending loads contribute to the corrosion of the CAW either alone or in combination by mimicking the clinical application. The results showed that the application of a mechanical strain significantly decreased the corrosion resistance of the CAW and increased the release of toxic corrosion products. The addition of the proteins inhibited the corrosion of the CAW, but the mechanical loads counteracted this effect. Mucin enhanced the corrosion resistance of the CAW. The effects of the proteins or strain, either alone or in combination, should be considered in the application of medical materials of heterogenetic alloys.



1. INTRODUCTION

Nickel titanium (NiTi) shape memory alloys and stainless steel (SS) arch wires have been used in orthodontic clinics for a long time. NiTi shape memory alloy (SMA) wire has superelastic properties, but its low stiffness easily causes movement of anchorage teeth. Though the stiffness of the SS arch wire provides enough anchorage, it can easily cause alveolar bone absorption.^{1–3} Composite arch wire (CAW) is a new type of orthodontic arch wire in which NiTi and SS wires are soldered with a Cu interlayer by laser welding. Their application could effectively reduce the pain and simplify clinical practice. Its joint bending angle and tensile strength could reach 180° and 520 MPa. Its shape recovery ratio reaches 98%,^{4–6} and it has sufficient corrosion resistance and decent biocompatibility in neutral, acidic, and fluoridated artificial saliva (AS).^{4,7,8}

Saliva plays a significant role in the lubrication and friction reduction due to the presence of phosphates, proteins, and bicarbonates.⁹ It is necessary to evaluate the corrosion resistance of biological alloys in the range of possible corrosive environments in actual use.¹⁰ The biocompatibility of implant alloys is strongly related to the interfacial kinetics including the release of metals and binding of proteins.^{10,11} Fibrinogen (Fb) is the coagulation factor with the highest concentration in the plasma, and the adsorption of Fb was considered a key factor in thrombus formation after the implantation of medical devices.^{12,13} It has the effect of mediating the subsequent adherence of cells on the surface of biomaterials.¹⁴ Mucins are a family of glycosylated proteins produced by epithelial tissues in the digestive and respiratory systems.^{15,16} A key characteristic of mucins in oral is that they form gels and participate in the occurrence of dental caries as chemical barriers. Salivary

analogues based on mucin have been considered ideal saliva substitutes.¹⁵ Immunoglobulin G (IgG) is one of the main antibody isotypes, produced by plasma cells. It accounts for about 75% of the total content of immunoglobulins in serum and can bind to many types of pathogens to protect the body from infection.¹⁷

In clinical applications, CAWs are under a continuous bending strain to correct misplaced teeth. It is important to explore the combined effect of proteins and bending strain on the corrosion resistance of laser welding CAWs with Cu interlayer. Moreover, the NiTi part of the CAW could release nickel ions due to corrosion, which may cause side reactions to local mucosal tissue or the whole body. The cytotoxicity of CAW under strain should also be studied. The objective of this study was to explore the effects of different proteins and continuous strain on the corrosion behavior, mechanisms, and cytotoxicity of CAWs in a simulated oral environment to provide a deep insight into their electrochemistry, topography, and cytotoxicity. The results of this study can be used as a reference for the improvement of promising CAWs and other advanced materials used in dentistry.

Received: February 23, 2020

Accepted: March 30, 2020

Published: April 9, 2020



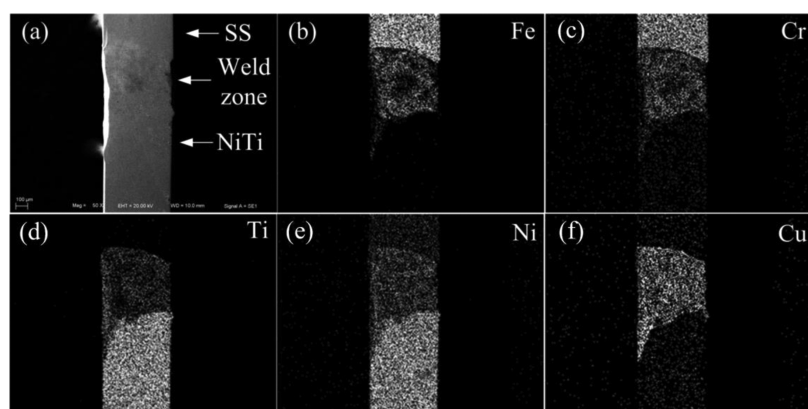


Figure 1. Representative SEM image of (a) the welded CAW surface and (b–f) EDS results of individual elements.

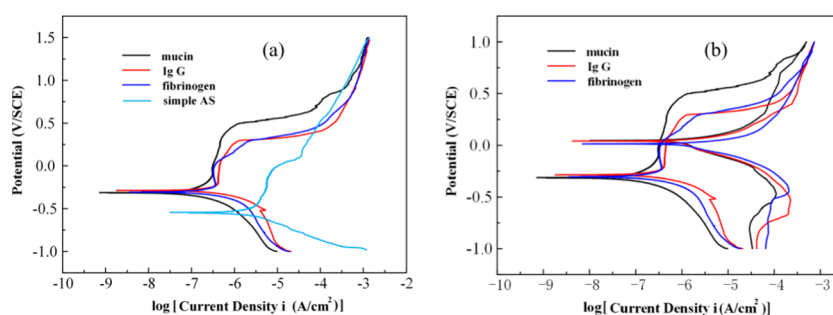


Figure 2. Potentiodynamic polarization behavior and typical cyclic polarization curves of CAW in different types of solutions: (a) polarization curves for the CAW in different solutions and (b) representative cyclic polarization curves of the CAW in different solutions.

2. RESULTS

2.1. Microstructures of the CAW Components. The NiTi and SS sections of the CAW were soldered together with an interlayer of pure Cu. Figure 1 shows the scanning electron microscopy (SEM) microstructures and energy-dispersive spectroscopy (EDS) components of the welding zone. The welding surface of Cu had a heterogeneous, smooth, and continuous appearance.

2.2. Electrochemical Measurements. The electrochemical behavior of the CAW is graphed in Figure 2, and the detailed parameters are calculated in Table 1. The corrosion

Table 1. $E_b - E_{\text{corr}}$, $E_b - E_{\text{prot}}$, and i_{corr} Values Calculated from the Potentiodynamic Polarization Curves^a

solution	$E_b - E_{\text{corr}}$ (mV/SCE)	$E_b - E_{\text{prot}}$ (mV/SCE)	i_{corr} ($\mu\text{A}/\text{cm}^2$)
simple AS	674 (± 23)		1.02 (± 0.09)
mucin	808 (± 29)	421 (± 16)	1.17 (± 0.18)
IgG	552 (± 17)	219 (± 14)	5.82 (± 0.35)
fibrinogen	398 (± 22)	75 (± 7)	5.97 (± 0.21)

^aData are presented as mean \pm standard deviation.

potentials (E_{corr}) of the protein groups were similar and higher than those of the simple AS. The values of the pitting potential (E_{pit}) in the protein solution groups were higher than that in the AS, and the E_{pit} in the mucin group was the highest among the groups herein. The value between the breaking potential (E_b) and E_{corr} ($E_b - E_{\text{corr}}$) in the mucin AS was the largest, whereas that in Fb AS was the smallest. The value of i_{corr} was higher in the protein groups than that in the simple AS. The value of i_{corr} in the mucin AS was the smallest among the

groups herein, and the values of E_{corr} and i_{corr} in the IgG AS were similar to those in the Fb group. The cyclic polarization behavior of the CAW presented a hysteresis as shown in Figure 2b. The value of $E_b - E_{\text{prot}}$ in the mucin group was the largest among the groups herein, and it was similar for the IgG AS and Fb AS.

2.3. Surface Morphology, Weight Loss, and Release of Cu after Immersion Test. After the immersion test, the surface morphology of the Cu interlayer of the CAWs was detected by SEM (Figure 3). The numbers and depths of the corrosion pits in the protein group seem smaller than those in the simple AS. However, the interlayer under bending strain showed a rougher and more irregular surface morphology than that of the unstrained samples in the same type of solution. As the applied load increased, the corrosion loci increased in length and depth. The corrosion morphologies appeared less rough in the mucin groups than in the other groups at the same load. In Figure 3h,k, the interface between the ruptured oxide layer and bare metal can also be seen. The corrosion pits consisted mostly of oxygen, carbon, calcium, and phosphorus. The microscopic morphologies of the interlayer determined by atomic force microscopy (AFM) (Figure 4) showed small and dense shallow corrosive pits in the mucin AS. The morphology of the IgG AS and Fb AS was rough with large particles of sediment accompanied by deep corrosion cracks.

The release of Cu and the weight loss were presented as percentages based on the specimen surface (Figure 5). With the increase of applied strain, the precipitation of copper ions increased, but the weight loss did not change substantially. The amounts of Cu release in the protein groups were smaller than that in the simple AS, and the smallest amount of Cu release among the protein groups was in the mucin group.

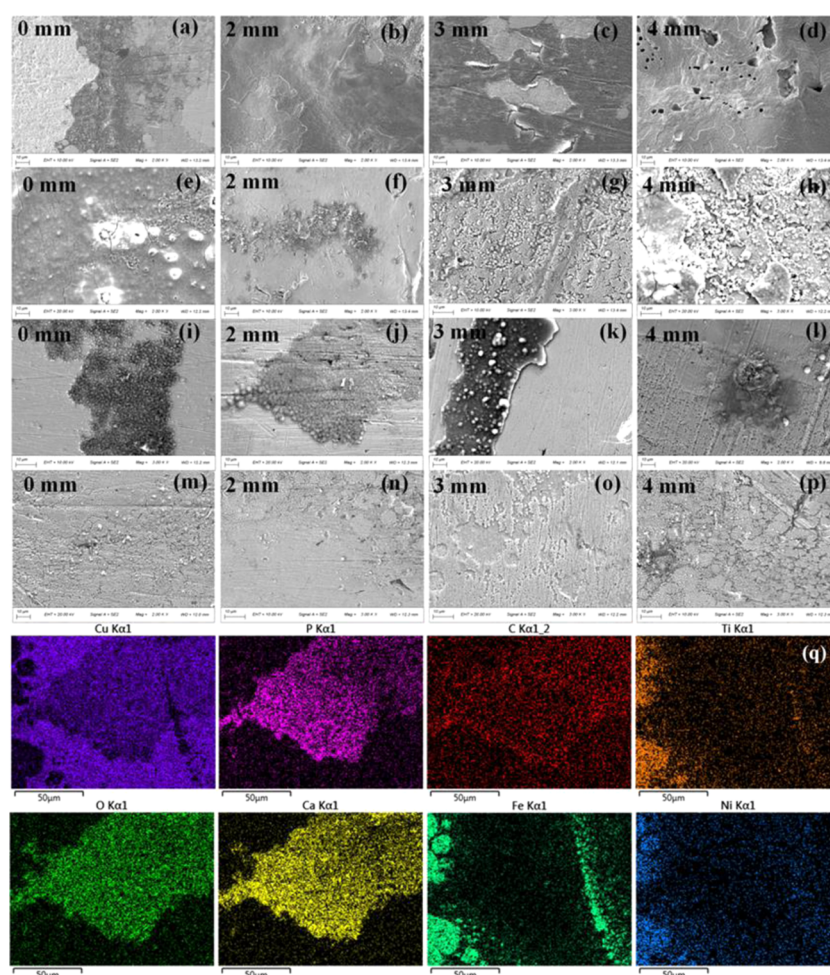


Figure 3. Representative SEM images showing the surface morphology and EDS results of the CAWs after immersion in the AS for 28 days with different types of proteins under the indicated loading conditions: (a–d) simple AS, (e–h) Fb AS, (i–l) IgG AS, (m–p) mucin AS, and (q) EDS analysis of (i).

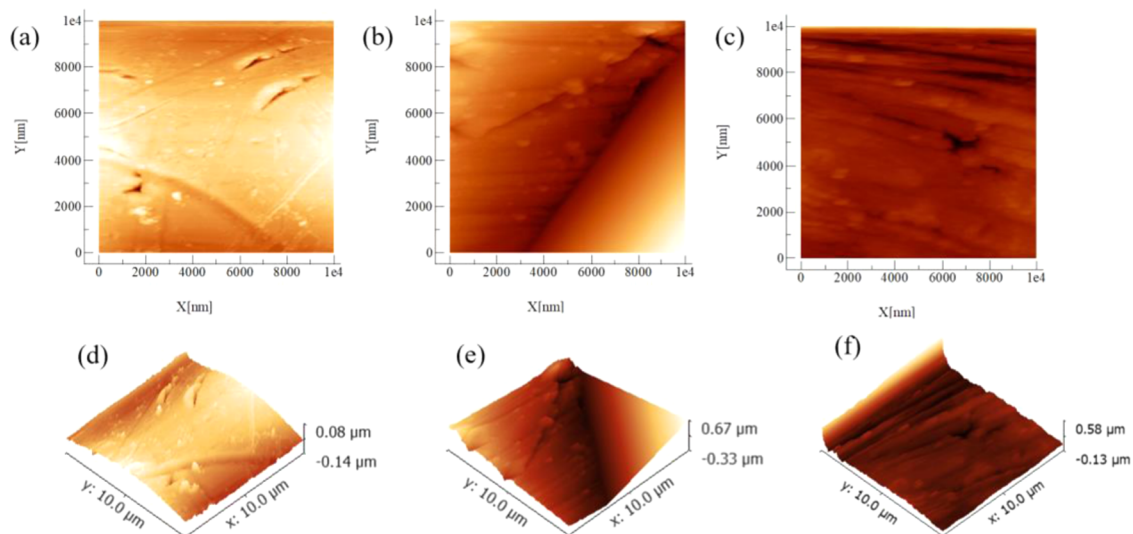


Figure 4. Two-dimensional (2D) and three-dimensional (3D) microscopic morphologies obtained by AFM of the CAW samples immersed in the protein solutions: (a) 2D image of mucin AS, (b) 2D image of IgG AS, (c) 2D image of Fb AS, and (d–f) 3D images of (a–c), respectively.

2.4. In Vitro Cytotoxicity of the CAW Extract. In vitro cytotoxicity of the CAW corrosion products was evaluated, and the relative cell viability was calculated and presented as

percentage (Figure 6). The viability of the control was considered to be 100%. The viability of the cells cultured with the protein extract decreased compared to that in the negative

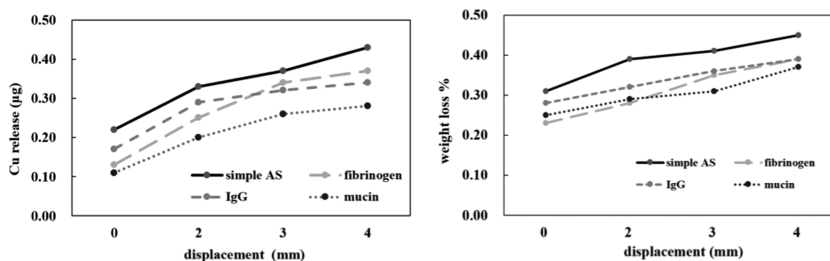


Figure 5. Release of elemental Cu analyzed by inductively coupled plasma optical emission spectrometry (ICP-OES) and the percentage of the weight loss of the samples based on the specimen surface after immersion.

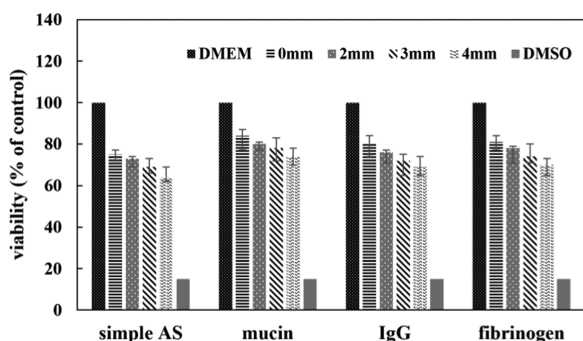


Figure 6. Relative viability of L-929 cells compared to that in the negative control (Dulbecco's modified Eagle medium (DMEM) only) after 48 h of culture in the CAW extraction media.

control but higher than that in the simple AS. The vitality decreased gradually as the applied load increased. The viability of the mucin was the highest among the protein groups under the same external strain, but the differences were not statistically significant. The viability cultured in the CAW protein extract maintained a level greater than 70% over 48 h.

3. DISCUSSION

Protein intake from food and the salivary secretion of digestive enzymes make saliva a complex system containing proteins. The strength and corrosion resistance of the Cu interlayer determined the clinical application performance of the CAW. The clinical application time of different sizes of arch wire is up

to 2 months generally, and the corrosion test period was set to be 60 days in this study and the performance of Cu interlayer was observed. The composition of the material, homogeneity of the microstructure, and surface morphology make the anticorrosion ability, elemental release, and cytotoxicity of biomedical materials different. The electrochemical performance, such as breakdown of the oxide layer, has been hindered in the presence of proteins.¹⁸ During electrochemical testing, the high values of E_{corr} in the protein groups indicated that the corrosion resistance was improved by protein.^{19,20} The highest E_{pit} of the mucin group suggested that the pitting corrosion tendency decreased in that solution. The largest $E_b - E_{\text{corr}}$ in the mucin AS further illustrated that the pitting corrosion stability was higher. The value of i_{corr} in the protein group was higher since the protein was an electrolyte and could contribute to the corrosion. The lowest i_{corr} value of the mucin AS indicates that the corrosion rate was the slowest among the protein groups. During cyclic polarization, the highest $E_b - E_{\text{prot}}$ of the mucin group and the lowest of the Fb group indicate that the repair capacity of the passive film in the mucin AS was strong, while that in the Fb AS was relatively weak.

After 60 days of immersion, the corrosion pits in the protein groups exhibited small and circumscribed loci, indicating that the corrosion resistance increased when the proteins were present. The weight loss was similar to that in the simple AS since the weight loss during corrosion might have been counteracted by the deposition of proteins on the surface. The release of Cu in the protein solution was smaller, which

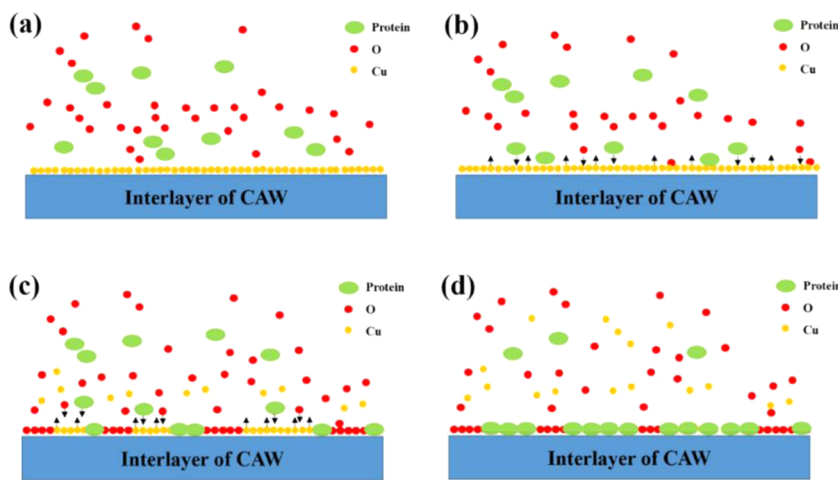


Figure 7. Schematic corrosion diagram of CAW in protein AS: (a) the protein participates in the corrosion process with oxygen; (b) the protein molecules compete with oxygen to bind copper ions; (c) the protein and oxygen participate in the formation of a passive layer and the Cu begins to dissolve; and (d) the protein and oxygen absorb and constitute the protective layer to prevent further Cu release from the interlayer of the CAW.

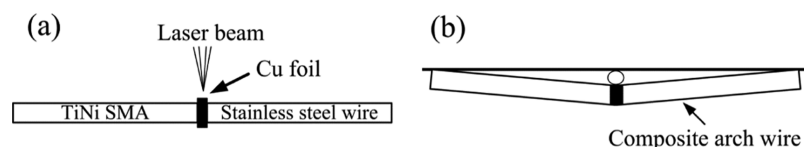


Figure 8. Schematic diagram of (a) the CAW assembly by laser welding and (b) the device used to apply three-point bending forces to the CAW samples.

suggested that the progress of corrosion was inhibited. Among the groups herein, the smallest ion release appeared in the mucin group, which further confirmed that the corrosion of the CAW in the mucin AS decreased. Other research found that mucin adsorption could decrease the metal release of stainless steel (AISI 316)²¹ and hinder the corrosion of an AZ31 magnesium alloy,²² which also agrees with our results.

Clinical observations have shown that frequent breakage happened in orthodontic wires because of the corrosion exposure in oral. The corrosion resistance of the alloys originated from both their anticorrosion ability and the self-healing capability of the passive layer. A bending strain could induce the deformation of the oxide film, generate an initial cracking point that then spreads along the wire, and provide space for H⁺ or other invasive ions to penetrate the material. Then, the damage would cause loss of this protection and allow corrosive solutions to react and erode the metal below. The cracks leave the metal underneath exposed and accelerate corrosion. The strain deformation accelerates the rupture and inhibits the process of self-healing or repair of the passive film, as demonstrated by the interface between the ruptured oxide layer and bare metal shown in Figure 3h,k. Therefore, this was the reason for the increase in the severity of the corrosion as the strain increased. According to AFM results, the oxide film deposited by the aggregation of the different proteins formed different morphologies, leading to different anticorrosion abilities of the CAWs.

According to the results, we elucidated how the proteins might interact with the corrosion process (Figure 7). In the simple AS without the proteins, the main component of the passive layer of the CAW was the oxide of Cu. During the formation of the oxide film, some of the calcium and phosphorus in the AS were simultaneously deposited.⁴ When the proteins participated in the corrosion process, they competed with the oxygen to bind copper ions. This is the reason for the increased dissolution of Cu and aggravated corrosion when the interface was exposed to a protein solution first. However, soon after the protein adsorbed and occupied the surface, the equilibrium of dissolution and adsorption was established. At this time, the interface was composed of a protein, oxygen, and copper. Of course, the following process was also accompanied by the deposition of calcium and phosphorus, while the areas with the deposition tended to form corrosive pits, due to the chelation and electrostatic adsorption of the protein molecules. Therefore, to a certain extent, the deposited film hindered the dissolution of copper below and played a protective role.

In cytotoxicity tests, the viability of cells cultured with corrosion products was all lower than that negative control but higher than that in the simple AS under the same external strain. The viability of the mucin group relatively increased, which indicates that mucin could reduce the toxic components to a certain extent. The vitality of cells decreased gradually as the applied load increased, which suggests that the corrosion

progress aggravated, and the amount of harmful corrosion products accumulated. In summary, the viability of the cells even under extreme strain remained greater than 60%, indicating that CAW was not highly toxic. By evaluating the toxicity of the corrosion products, not only the biosafety could be evaluated but also the corrosion process of CAW could be speculated. This provides a new path and reference for the biocompatibility detection and surface modification of medical materials. The results in this study provide foundational information to predict the corrosion behavior of CAWs under the dual effects of protein exposure and bending strain for future in vivo studies.

4. CONCLUSIONS

The corrosion resistance of the CAW was improved by the presence of the proteins. The repair capacity of the passive film on the surface in the mucin AS was strong, while that in the Fb was relatively weak. The toxicity of the corrosion extract was aggravated as the strain increased. The addition of mucin partly inhibited the progress of the corrosion and reduced the toxicity of the corrosion products. Under the combination of protein exposure and strain loads, the CAW demonstrated a considerable corrosion resistance to complete clinical function.

5. EXPERIMENTAL SECTION

5.1. Materials and Sample Preparation. The base metals in this investigation were Ti–44.73 wt % NiTi SMA wire and Fe–18Cr–8Ni SS. The dimensions of the wires were 25 mm (length) × 0.64 mm (width) × 0.48 mm (thickness). The wires were placed on an end-to-end welding fixture with pure Cu as the interlayer and welded by a Nd:YAG laser welding system (JHM-1GY 300B), as described in a previous study (Figure 8a).^{4–8}

5.2. Test Solution Preparation, Immersion Tests, and Strain Conditions. The components in the AS were prepared as described in a previous study.^{6–8} The concentration of Fb, IgG, and mucin (Sigma) was 40 mg/L. A three-point flexure fixture fabricated from a glass sheet was used to apply a continuous three-point bending force to the interlayer of the CAW (Figure 8b). The device was deflected to displacements of 2.0, 3.0, and 4.0 mm to mimic the application of the strain from the bending stress when correcting malposed teeth. The free length of the arch wires was 50 mm. Each experiment contained 12 groups [three types of protein (Fb, IgG, and mucin) × four loading strain (bending distances of 0, 2.0, 3.0, and 4.0 mm)], and there were six replicates of each group. The wires were immersed and maintained at 37 °C. After 60 days, the samples were weighed and the weight loss was calculated. The immersed solutions were collected for metal-ion detection by inductively coupled plasma optical emission spectrometry (ICP-OES) and cell cytotoxicity tests.

5.3. Electrochemical Measurements. The CHI 920C electrochemical workstation was used, and the counter electrode and the reference electrode were a platinum plate

and saturated calomel electrode (SCE), respectively. The exposed area for the test was $20 \times 0.64 \text{ mm}^2$. The electrochemical cell was immersed in a water bath to maintain the temperature at $37 \pm 0.5 \text{ }^\circ\text{C}$. The scan started from -1 V/SCE with a sweep rate of 1 mV/s .²³

5.4. Scanning Electron Microscopy Observation of the Surface Morphologies. After the immersion corrosion, the surface morphology of the Cu interlayer was observed using an environmental SEM. The topographical characterization of the specimens was recorded by atomic force microscopy (AFM).

5.5. Cytotoxicity Testing In Vitro. The mouse fibroblast L-929 cell line was cultured at $37 \text{ }^\circ\text{C}$ and $5\% \text{ CO}_2$ to evaluate the cytotoxicity. The culture medium was Dulbecco's modified Eagle's medium (DMEM) with 10% fetal bovine serum, 100 U/mL penicillin, and $100 \text{ } \mu\text{g/mL}$ streptomycin. The solutions containing corrosion products after immersion testing were sterilized by UV irradiation for 1 h as the CAW extract. Then, part of the medium was replaced with $20 \text{ } \mu\text{L}$ of corrosive solution. Simple DMEM was used as a negative control, and dimethyl sulfoxide (DMSO) was used as a positive control.⁷ After incubation for 48 h , the activity of cell proliferation was evaluated by the cell counting kit-8 (CCK-8) test (Dojindo Molecular Technologies, Japan). The spectrophotometric absorbance was measured at 490 nm by a microplate reader (Molecular Devices). The viabilities of the cells were calculated as mean \pm standard deviation with $n = 5$ per group.

AUTHOR INFORMATION

Corresponding Author

Chao Zhang – Orthodontic Department, Stomatological Hospital, Southern Medical University, Guangzhou 510280, China; orcid.org/0000-0002-7652-923X; Phone: +86 18565578907; Email: 2645491781@qq.com

Authors

Longwen He – Orthodontic Department, Stomatological Hospital, Southern Medical University, Guangzhou 510280, China

Ye Cui – Orthodontic Department, Stomatological Hospital, Southern Medical University, Guangzhou 510280, China

Complete contact information is available at:

<https://pubs.acs.org/10.1021/acsomega.0c00803>

Author Contributions

The main contribution of C.Z. is experimental design. Y.C. and L.H. carried out measurements together, and the manuscript composition is completed by L.H.

Notes

The authors declare no competing financial interest.

ACKNOWLEDGMENTS

This work was funded by the National Natural Science Foundation of China (81801007), Postdoctoral Science Foundation of China (2019M652980), Natural Science Foundation of Guangdong Province (2018A030310442), and Science and Cultivation Foundation of Stomatological Hospital of Southern Medical University (PY2018027).

REFERENCES

(1) Toker, S. M.; Canadinc, D. Evaluation of the biocompatibility of NiTi dental wires: a comparison of laboratory experiments and clinical conditions. *Mater. Sci. Eng., C* **2014**, *40*, 142–147.

(2) Kusy, R. P. A review of contemporary archwires: their properties and characteristics. *Angle Orthod.* **1997**, *67*, 197–207.

(3) Kuntz, M. L.; Vadori, R.; Khan, M. I. Review of Superelastic Differential Force Archwires for Producing Ideal Orthodontic Forces: an Advanced Technology Potentially Applicable to Orthognathic Surgery and Orthopedics. *Curr. Osteoporosis Rep.* **2018**, *16*, 380–386.

(4) Zhang, C.; Sun, X.; Hou, X.; Li, H.; Sun, D. The corrosion resistance of composite arch wire laser-welded by NiTi shape memory alloy and stainless steel wires with Cu interlayer in artificial saliva with protein. *Int. J. Med. Sci.* **2013**, *10*, 1068–1072.

(5) Sun, D. Q.; Li, H. M. A new method of TiNi shape memory alloy and austenitic stainless steel different Kind of material connection. Patent number CN21520172011.

(6) Zhang, C.; Liu, J.; Yu, W.; Sun, D.; Sun, X. Susceptibility to corrosion of laser welding composite arch wire in artificial saliva of salivary amylase and pancreatic amylase. *Mater. Sci. Eng., C* **2015**, *55*, 267–271.

(7) Zhang, C.; Sun, X.; Zhao, S.; Yu, W.; Sun, D. Susceptibility to corrosion and in vitro biocompatibility of a laser-welded composite orthodontic arch wire. *Ann. Biomed. Eng.* **2014**, *42*, 222–230.

(8) Zhang, C.; Zhao, S.; Sun, X. M.; Sun, D. Q.; Sun, X. H. Corrosion of laser-welded NiTi shape memory alloy and stainless steel composite wires with a copper interlayer upon exposure to fluoride and mechanical stress. *Corros. Sci.* **2014**, *82*, 404–409.

(9) Zeng, Q.; Zheng, J.; Yang, D.; Tang, Y.; Zhou, Z. Effect of calcium ions on the adsorption and lubrication behavior of salivary proteins on human tooth enamel surface. *J. Mech. Behav. Biomed. Mater.* **2019**, *98*, 172–178.

(10) Hedberg, Y. S.; Dobryden, I.; Chaudhary, H.; Wei, Z.; Claesson, P. M.; Lendel, C. Synergistic effects of metal-induced aggregation of human serum albumin. *Colloids Surf., B* **2019**, *173*, 751–758.

(11) Höhlinger, M.; Christa, D.; Zimmermann, V.; Heise, S.; Boccaccini, A. R.; Virtanen, S. Influence of proteins on the corrosion behavior of a chitosan-bioactive glass coated magnesium alloy. *Mater. Sci. Eng., C* **2019**, *100*, 706–714.

(12) Guo, L.; Liang, C.; Guo, H.; Chen, W. Effect of fibrinogen on corrosion behavior of stainless steel in artificial blood solution. *J. Biomed. Eng.* **2001**, *18*, 565–567.

(13) Chao, Z.; Yaomu, X.; Chufeng, L.; Conghua, L. The effect of mucin, fibrinogen and IgG on the corrosion behaviour of Ni-Ti alloy and stainless steel. *BioMetals* **2017**, *30*, 367–377.

(14) Huo, W. T.; Zhao, L. Z.; Zhang, W.; Lu, J. W.; Zhao, Y. Q.; Zhang, Y. S. In vitro corrosion behavior and biocompatibility of nanostructured Ti6Al4V. *Mater. Sci. Eng., C* **2018**, *92*, 268–279.

(15) Mystkowska, J.; Car, H.; Dąbrowski, J. R.; Romanowska, J.; Klekotka, M.; Milewska, A. J. Artificial Mucin-based Saliva Preparations - Physicochemical and Tribological Properties. *Oral Health Prev. Dent.* **2018**, *16*, 183–193.

(16) Yan, H.; Chircov, C.; Zhong, X.; Winkeljann, B.; Dobryden, I.; Nilsson, H. E.; Lieleg, O.; Claesson, P. M.; Hedberg, Y.; Crouzier, T. Reversible Condensation of Mucins into Nanoparticles. *Langmuir* **2018**, *34*, 13615–13625.

(17) Kapur, R.; Einarsdottir, H. K.; Vidarsson, G. IgG-effector functions: “the good, the bad and the ugly”. *Immunol. Lett.* **2014**, *160*, 139–144.

(18) Rituerto Sin, J.; Neville, A.; Emami, N. Corrosion and tribocorrosion of hafnium in simulated body fluids. *J. Biomed. Mater. Res., Part B* **2014**, *102*, 1157–1164.

(19) Pound, B. G. The use of electrochemical techniques to evaluate the corrosion performance of metallic biomedical materials and devices. *J. Biomed. Mater. Res., Part B* **2019**, *107*, 1189–1198.

(20) Prando, D.; Brenna, A.; Diamanti, M. V.; Beretta, S.; Bolzoni, F.; Ormellese, M.; Pedferri, M. Corrosion of titanium: Part 1: aggressive environments and main forms of degradation. *J. Appl. Biomater. Funct. Mater.* **2017**, *15*, e291–e302.

(21) Lundin, M.; Hedberg, Y.; Jiang, T.; Herting, G.; Wang, X.; Thormann, E.; Blomberg, E.; Wallinder, I. O. Adsorption and protein-

induced metal release from chromium metal and stainless steel. *J. Colloid Interface Sci.* **2012**, 366, 155–164.

(22) Jang, Y.; Owuor, D.; Waterman, J. T.; White, L.; Collins, B.; Sankar, J.; Gilbert, T. W.; Yun, Y. Effect of Mucin and Bicarbonate Ion on Corrosion Behavior of AZ31 Magnesium Alloy for Airway Stents. *Materials* **2014**, 7, 5866–5882.

(23) ASTM Standard F 2129-06. *Standard Test Method for Conducting Cyclic Potentiodynamic Polarization Measurements to Determine the Corrosion Susceptibility of Small Implant Devices*, ASTM International: West Conshohocken, Pennsylvania, 2006.